catalysts

MDPI

Article

Synthesis, Characterization and Enhanced Visible Light Photocatalytic Performance of $ZnWO_4$-NPs@rGO Nanocomposites

Norah Alhokbany *, Saad M. Alshehri and Jahangeer Ahmed *

Department of Chemistry, College of Science, King Saud University, Riyadh 11451, Saudi Arabia; alshehri@ksu.edu.sa

* Correspondence: nhokbany@ksu.edu.sa (N.A.); jahmed@ksu.edu.sa (J.A.)

Abstract: $ZnWO_4$ nanoparticles on reduced graphene oxide ($ZnWO_4$-NPs@rGO) nanocomposites were synthesized using the hydrothermal method. Structural, morphological, optical, and photocatalytic studies of the $ZnWO_4$-NPs@rGO nanocomposites were successfully investigated. Photocatalytic performances of the $ZnWO_4$-NPs@rGO nanocomposites were examined for the degradation of hazardous methylene blue dye (HMBD) in a neutral medium. $ZnWO_4$-NPs@rGO nanocomposites show superior photo-catalytic performances over pure $ZnWO_4$ nanoparticles. $ZnWO_4$-NPs@rGO nanocomposites degrade ~98% dye while pure $ZnWO_4$ nanoparticles degrade ~53% dye in 120 min. The prepared nanocomposites also show excellent recycled photo-catalytic efficiencies over multiple cycles.

Keywords: $ZnWO_4$-NPs@rGO; nanocomposites; photo-catalysis; degradation

Citation: Alhokbany, N.; Alshehri, S.M.; Ahmed, J. Synthesis, Characterization and Enhanced Visible Light Photocatalytic Performance of $ZnWO_4$-NPs@rGO Nanocomposites. *Catalysts* **2021**, *11*, 1536. https://doi.org/10.3390/catal11121536

Academic Editors: Zsolt Pap, Lucian Baia and Monica Baia

Received: 15 November 2021
Accepted: 14 December 2021
Published: 16 December 2021

1. Introduction

The recycling of catalysts for multifunctional purposes is currently receiving the attention of scientists, to reduce the cost of commercial materials for a diverse range of technological uses. In this paper, we focus on the catalytic efficiency of reused cost-effective materials for various applications. It is noteworthy that the compounds belonging to group VI-B (including tungsten) showed tremendous efficiencies in various applications including as photo-catalysis [1–4], electro-catalysis [5,6], and for energy storage [7,8]. The treatment of contaminated water is an important way to regulate health issues by removing organic pollutants from water through the photo-catalytic process. Photo-catalysis is one of the promising methods for environmental remediation. Semiconductor-based nanocomposite materials were investigated as low-cost and high-performance photo-catalysts to control water pollution problems [9–13]. Zinc tungstate ($ZnWO_4$) has large band gap energy (3.5–3.7 eV) and is used as an efficient photo-catalyst in the degradation of organic dyes under ultraviolet (UV) radiation [1,14]. $ZnWO_4$ nanostructured materials used as photo-catalysts were also previously reported to degrade dyes [15–19]. However, the recombination of charge carriers in these materials is a challenge for researchers. Therefore, loading heteroatoms, carbon-based materials, or transition metal ions into a $ZnWO_4$ matrix could be helpful for achieving efficient charge separation in semiconductors to improve their photocatalytic performance. The amalgamation of WO_3 and $ZnWO_4$ nanocomposites has enabled the achievement of efficient electron-hole charge separation, resulting in their reporting as efficient photo-catalysts [13,20]. Recently, $Ag/ZnWO_4$ nanocomposites have shown promising efficiencies in the degradation of methyl orange (MO) and methylene blue (MB) dyes under UV irradiation [21,22]. $ZnWO_4$ nanostructured materials have also been used for a range of purposes including for the extraction of dyes and heavy metals [23–25], as bacterial disinfectants [23], and for their photoluminescence [26], alongside being used as components in lithium-ion batteries [27,28] and supercapacitors [29,30]. Nevertheless,

some reports state that dyes are not appropriate molecules for visible-light degradation reactions because they can absorb light and desensitize the photo-catalysts [31,32]. Previously, we have designed various transition metal tungstate, molybdate, gallate, and ferrite nanostructured materials for a variety of applications including wastewater treatment [1,2], electro-catalysis [1,5,33–37], and supercapacitor [1,33,38] applications. Functionalization of the semiconducting nanoparticles with materials that have high electrical conductivities and surface areas is an interest of researchers for the effective improvement of the catalytic activities and stabilities of low-cost photo-catalysts. Graphene-based zinc oxide [39–41] nanocomposites were previously reported as promising photo-catalysts in organic dye degradation reactions. Therefore, we have designed nanocomposites containing rGO sheet-supported $ZnWO_4$ nanoparticles ($ZnWO_4$-NPs@rGO) for superior photocatalytic activities in neutral media. Recently, nickel molybdenum oxide nano-rods were initially used as photo-catalysts, and thereafter reused as efficient catalysts in electrochemical sensing and energy storage applications [42]. This report is mainly focused on the synthesis, characterization, and enhanced visible-light photo-catalytic efficiencies of the synthesized $ZnWO_4$-NPs@rGO nanocomposites.

2. Materials and Methods

2.1. Preparation of $ZnWO_4$ Nanoparticles

$ZnWO_4$ nanoparticles were initially synthesized using a solvent-free method (i.e., using molten salts) as reported elsewhere [1]. To prepare $ZnWO_4$ nanoparticles, one mole of $Zn(NO_3)_2{\cdot}6H_2O$ (Sigma Aldrich, 99%), one mole of $Na_2WO_4{\cdot}2H_2O$ (Sigma Aldrich, 99%), thirty moles of $NaNO_3$ (Sigma Aldrich, 98 + %), and thirty moles of KNO_3 (Sigma Aldrich, 99%) were taken and mixed homogeneously by grinding properly, and then heated at 500 ± 10 °C for 6 h in a muffle furnace. White-colored nano-powder was collected and washed with de-ionized water to remove the impurities. The resulting nanoparticles were dried at 50 °C. The phase purity of the prepared nanoparticles was analyzed by powder X-ray diffraction (XRD) studies using a Bruker D-8 Advanced diffractometer with Cu-Kα radiation.

2.2. Preparation of $ZnWO_4$-NPs@rGO Nanocomposites

The prepared $ZnWO_4$ nanoparticles and commercially available reduced graphene oxides (rGO, Sigma Aldrich) were taken in an appropriate ratio, followed by dispersion in de-ionized water (18 mL) and ethylene glycol (2 mL) via sonication for twenty min. The suspension was then transferred into an autoclave and treated via the hydrothermal method at 120 °C for 48 h. Dark grey-colored $ZnWO_4$-NPs@rGO nanocomposites were collected through centrifugation and then dried at 60 °C.

2.3. Characterization

The structural characterization of the prepared $ZnWO_4$-NPs@rGO nanocomposites was undertaken by powder X-ray diffraction (XRD), Fourier-transform infrared spectroscopy (FTIR, Bruker TENSOR-27), and X-ray photoelectron spectroscopy (XPS, PHI-5300). The surface morphologies and elemental compositions were evaluated by field emission scanning electron microscope (FESEM, JEOL, JSM-7600F) and energy dispersive studies (EDS). The optical band gap energy of $ZnWO_4$-NPs@rGO nanocomposites was determined using UV–Vis absorption spectra (Shimadzu-2550 spectrophotometer).

2.4. Photocatalytic Studies

The photocatalytic performance of $ZnWO_4$-NPs@rGO nanocomposites was measured by the degradation of a hazardous methylene blue dye (HMBD) solution. The Xenon lamp (400 W) with λ of ~400 nm was used as the visible light source for irradiation of the HMBD solution. 50 mg of $ZnWO_4$-NPs@rGO photo-catalyst was taken with 20 mL aqueous HMBD solution followed by stirring for 30 min to confirm the adsorption/desorption equilibrium. The photocatalytic degradation of the HMBD solution was investigated in

a neutral medium (pH ~7) at the λ_{max} of ~662 nm. Samples of the suspension measuring 2.0 mL (with maximum transparency) were taken at regular time intervals for the photocatalytic analysis. Note that the regeneration efficiency of the $ZnWO_4$-NPs@rGO photocatalyst was also investigated using similar experimental conditions as explained above. The mass spectrometry (MS) method for measuring dye degradation using photo-catalysts was also performed using an Agilent HPLC 1200 connected to a triple quadrupole mass spectrometer (Agilent 6410 QqQ) using a direct injection connector instead of a column. Detection was performed on a QqQ MS detector operated with an electrospray ionization (ESI) source. Low purity N_2 gas was used as drying gas with a flow rate of 12 L min^{-1}, and high purity N_2 gas as collision gas at a pressure of 60 psi. Source temperature and capillary voltage were set at 350 °C and 4000 V, respectively. Fragmentor voltage was set at 110 V with collision energy of 15 V.

3. Results and Discussion

The phases and crystalline structures of the prepared $ZnWO_4$-NPs@rGO nanocomposites were initially analyzed by XRD. Figure 1a shows the XRD patterns of the $ZnWO_4$-NPs@rGO nanocomposites, and all the reflections including the (011), (110), (111), (021), (200), (121), (112), (211), (022), (220), (130), (202), (113), (311), and (041) planes can be identified for the monoclinic phase of $ZnWO_4$ (JCPDS # 15–774). The resulting XRD patterns also agree with previous reports [1]. The additional XRD peaks (as marked by an *) represent rGO. No other peaks based on Zn or W oxides were detected in the XRD patterns, which confirmed the formation of $ZnWO_4$-NPs@rGO nanocomposites. Figure 1b shows the FTIR spectrum of the $ZnWO_4$-NPs@rGO nanocomposites. FTIR bands at low wavenumbers confirm the presence of $ZnWO_4$. FTIR bands at ~620 and ~850 cm^{-1} represent Zn-O-Zn and W-O bonds, respectively. FTIR bands at ~3500 and ~1650 cm^{-1} belong to the −OH groups from atmospheric moisture. FTIR bands at ~1220 and ~1570 cm^{-1} could be identified as the C=O and C-H vibrations of rGO, respectively, as supported by previous reports [5].

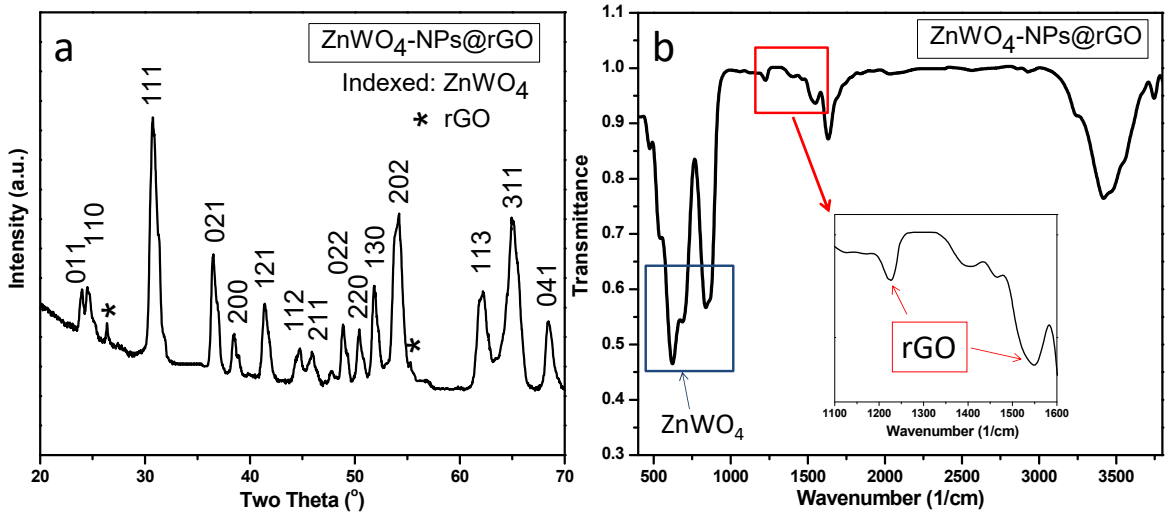

Figure 1. (**a**) XRD patterns and (**b**) FTIR spectrum of synthesized $ZnWO_4$-NPs@rGO nanocomposites.

FESEM measurements were taken at different magnifications to understand the morphology of the $ZnWO_4$-NPs@rGO nanocomposites (Figure 2). The FESEM micrographs clearly show that the $ZnWO_4$ nanoparticles are very well supported by the rGO sheets (Figure 2a,c). A careful visualization for particle size analysis was also studied at high magnification, and the average particle diameter of the $ZnWO_4$ nanoparticles was found to be ~50 nm (Figure 2d). Energy dispersive spectroscopy (EDS) equipped with FESEM was employed for the compositional analysis of the $ZnWO_4$-NPs@rGO nanocomposites (Figure 3). The EDS study revealed the presence of the chemical elements (i.e., Zn, W, O, and C) in the $ZnWO_4$-NPs@rGO nanocomposites as expected (Figure 3). The atomic % compositions

of Zn and W were found to be in a 1:1 ratio, in agreement with the initial 1:1 loaded stoichiometry. The XPS study was also further investigated to determine the elemental composition and chemical states of the $ZnWO_4$-NPs@rGO nanocomposites. Figure 4 shows a high-resolution XPS spectra of Zn (2p), W (4f), O (1s), and C (1s) in the $ZnWO_4$-NPs@rGO nanocomposites. Figure 4a shows the high-resolution XPS spectrum of Zn (2p). The XPS spectrum shows two peaks at ~1025 eV and 1048 eV, which are attributed to Zn (2p3/2) and Zn (2p1/2), respectively, and suggest the presence of a Zn^{2+} chemical state. Figure 4b shows the high-resolution XPS spectrum of W (4f). It shows two spin-orbit doublet peaks at ~35.25 eV and ~37.20 eV, which represent W (4f7/2) and W (4f5/2), respectively, in the W^{6+} chemical state. Figure 4c shows the high-resolution XPS spectrum of O (1s). The resulting O (1s) peak at ~532.7 eV was deconvoluted into two peaks at 532.8 and 533.9 eV, of Zn–O and W–O, respectively. A high-resolution XPS spectrum of C (1s) is shown in Figure 4d. A peak of C (1s) appeared at ~284.40 eV and deconvoluted into four peaks of C=C at ~284.22 eV, C-OH at ~284.44 eV, C-O-C at ~285.90 eV, and C=O at ~286.30 eV. It is noteworthy that the above characterization techniques strongly support the formation of $ZnWO_4$-NPs@rGO nanocomposites. Thereafter, the prepared nanocomposites were used as photo-catalysts in the degradation of organic pollutants into inorganic minerals under visible-light irradiation.

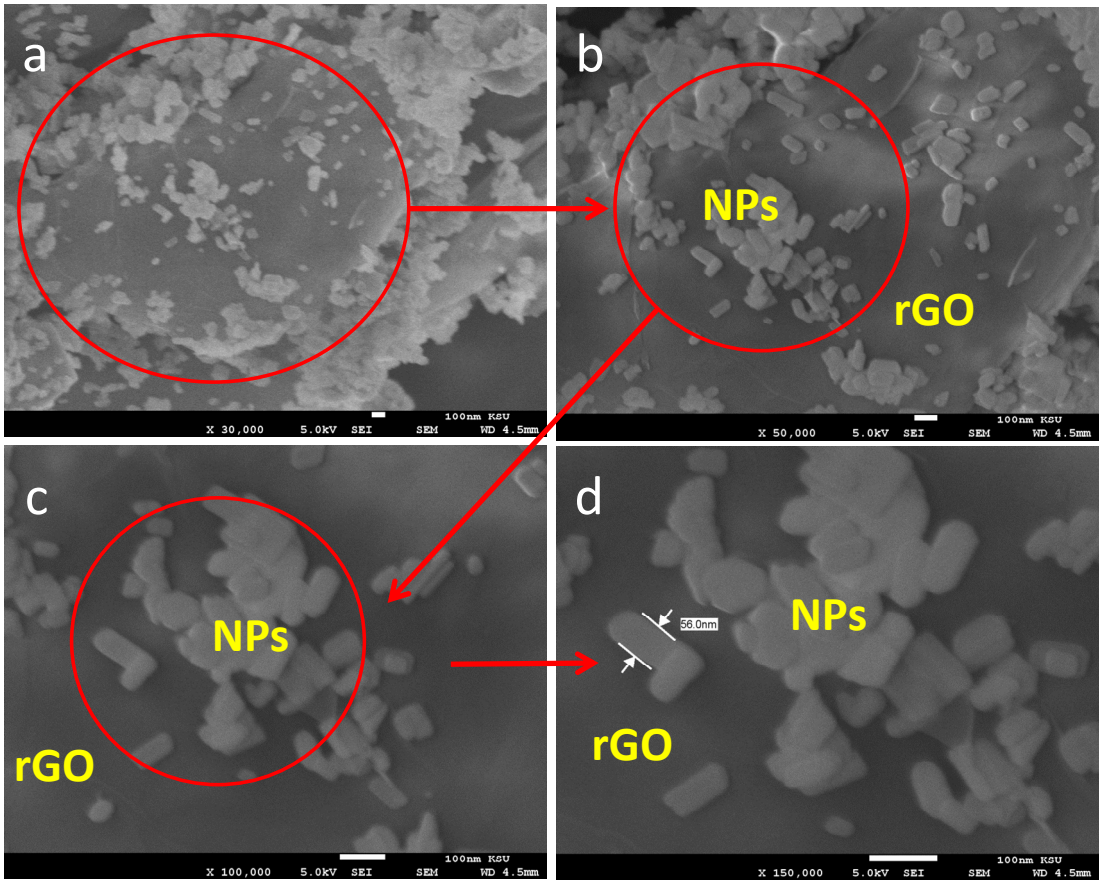

Figure 2. FESEM micrographs of $ZnWO_4$-NPs@rGO nanocomposites at (**a**,**b**) low and (**c**,**d**) high magnifications.

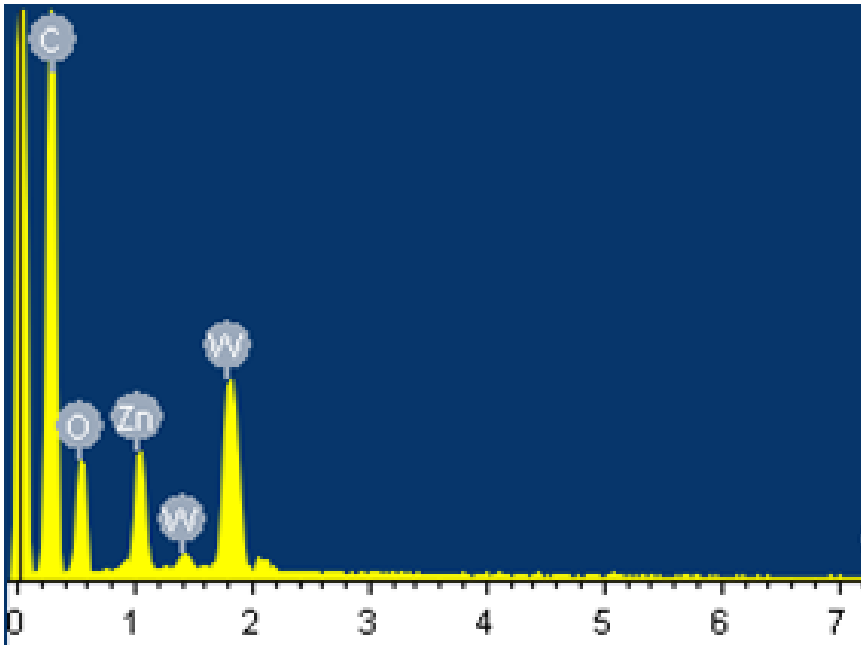

Figure 3. EDS study of $ZnWO_4$-NPs@rGO nanocomposites for elemental analysis.

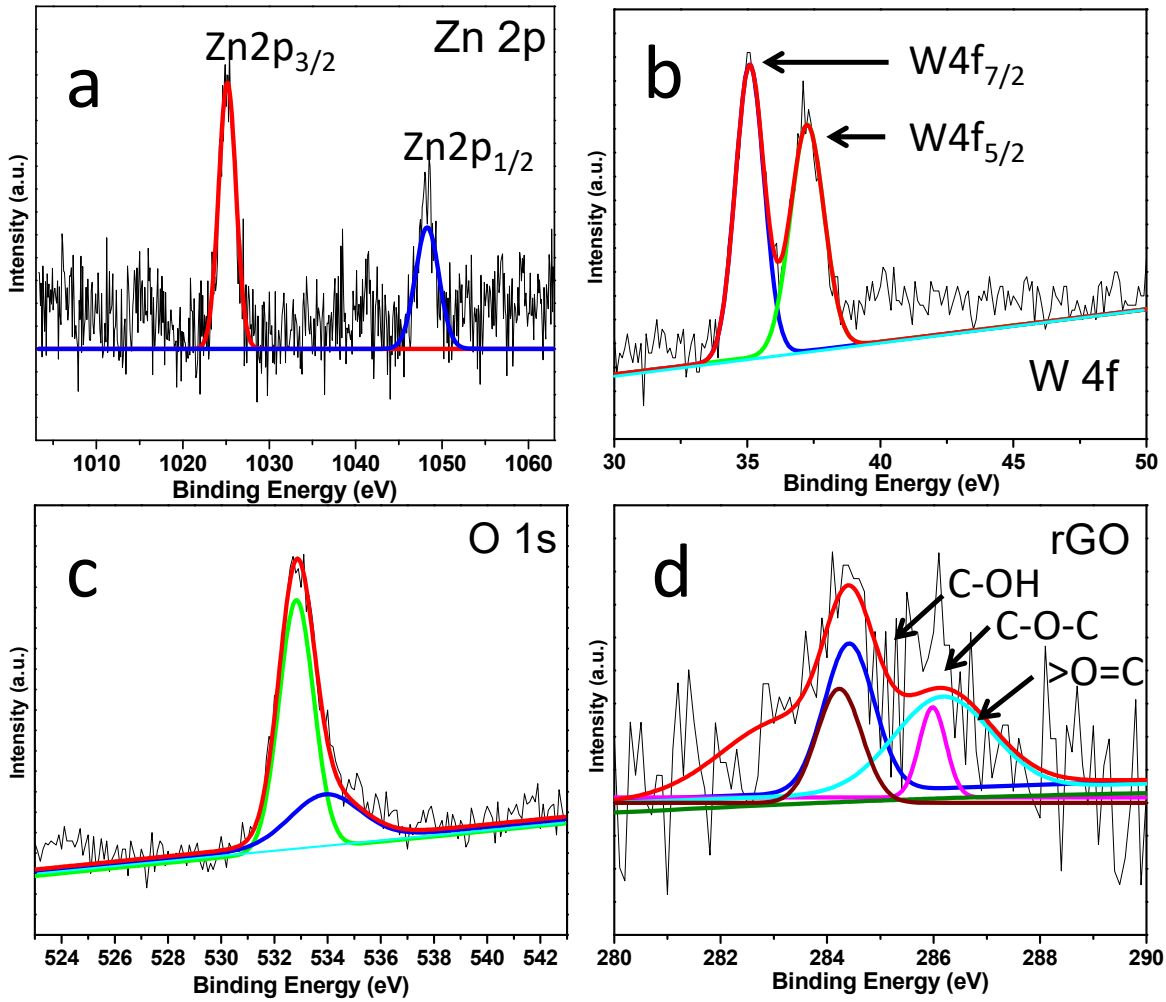

Figure 4. High-resolution XPS spectra of (**a**) Zn (2p), (**b**) W (4f), (**c**) O (1s), and (**d**) C (1s) in $ZnWO_4$-NPs@rGO nanocomposites.

The optical properties of $ZnWO_4$-NPs@rGO nanocomposites were also examined using UV–Vis absorption studies. The absorbance data of the $ZnWO_4$-NPs@rGO nanocomposites were recorded in the region from 100 to 900 nm (Figure 5). The optical band gap of the $ZnWO_4$-NPs@rGO nanocomposites was calculated using the absorption data, followed by use of Tauc's model [43]. The band gap energy of the $ZnWO_4$-NPs@rGO nanocomposites was found to be ~3.50 eV, as shown in the inset of Figure 5. The resulting band gap energy of the $ZnWO_4$-NPs@rGO nanocomposites was lower than that of pure $ZnWO_4$ materials (i.e., ~3.8 eV), as reported elsewhere [44]. Figure 6a shows the mechanism of photo-catalytic degradation of the HMBD solution into inorganic minerals under visible-light irradiation in the presence of the $ZnWO_4$-NPs@rGO nanocomposites. Photo-catalytic degradation of HMBD could be accompanied by the transfer of electrons from the valence band (VB) to the conduction band (CB) to form the electron (e^-)–hole (h^+) pairs. The e^-–h^+ pairs generate the $O_2{}^{-\bullet}$ and $OH^\bullet$ radicals, followed by the attack on HMBD to oxidize it into the form of inorganic minerals (e.g., $NH_4{}^+$, H_2O, CO_2, etc.). The reaction mechanism of hazardous methylene blue dye (HMBD) degradation could be summarized with the given mechanistic steps:

Photo-catalyst + hυ → Photo-catalyst (e^- + h^+) → Photo-catalyst + H^+ + $OH^\bullet$ + $O_2{}^{\bullet-}$

Photo-catalyst (h^+) + OH^- → Photo-catalyst + $OH^\bullet$

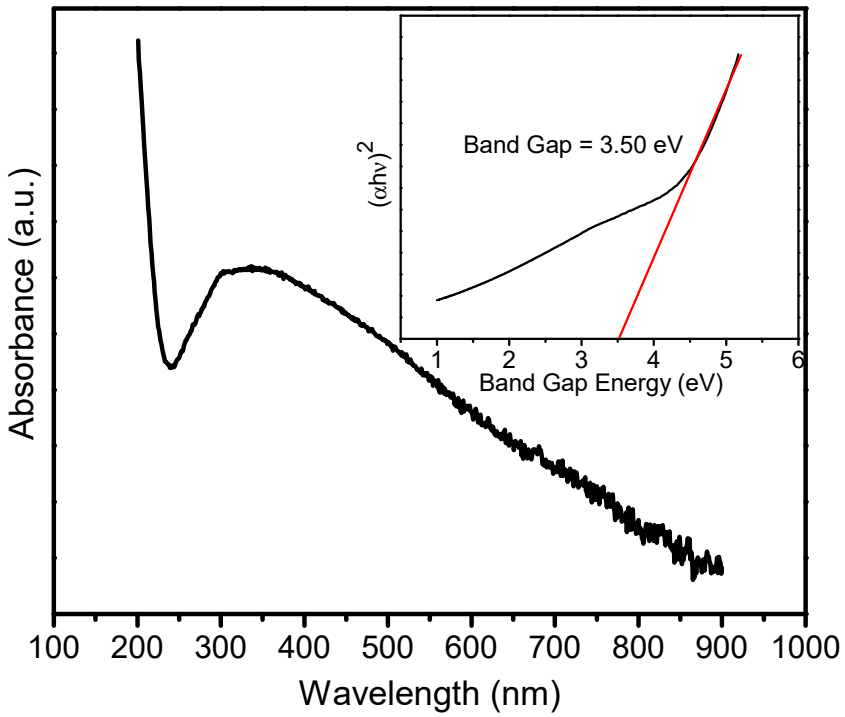

Figure 5. UV–Vis absorption spectrum of $ZnWO_4$-NPs@rGO nanocomposites. Inset shows the band gap energy of $ZnWO_4$-NPs@rGO nanocomposites.

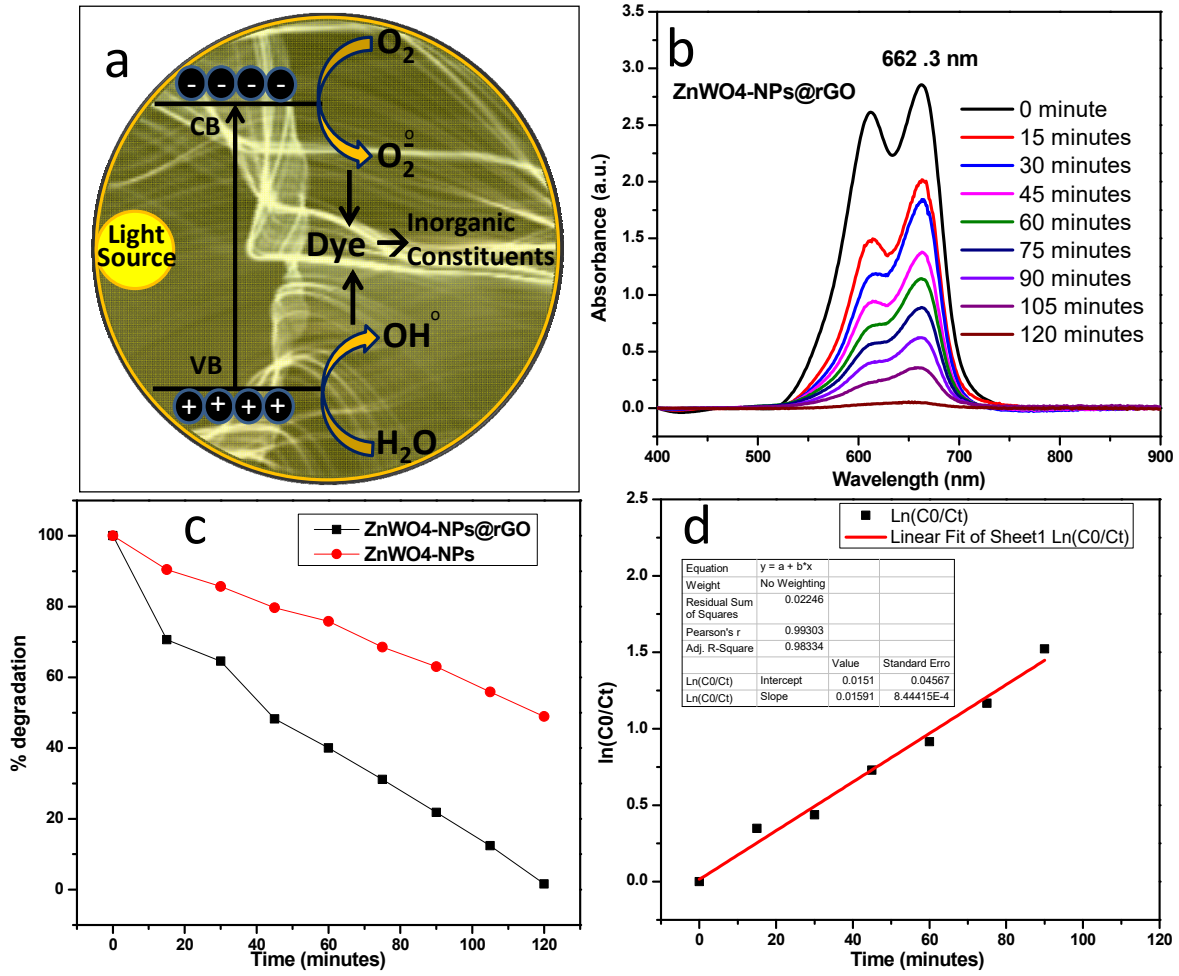

Figure 6. (**a**) Reaction scheme, (**b**) absorption spectra, (**c**) percent degradation, and (**d**) linear plot of photo-degradation of HMBD using $ZnWO_4$-NPs@rGO nanocomposites.

The electrons of photo-catalyst reduce the molecular O_2 to superoxide ($O_2^{\bullet -}$) at CB:

Photo-catalyst + O_2 + e^- → Photo-catalyst + $O_2^{\bullet}$

$O_2^{\bullet -}$ + H^+ → $HO_2^{\bullet}$

Formation of H_2O_2 followed by further reduction:

$2HO_2^{\bullet -}$ → H_2O_2 + O_2

H_2O_2 + e^- → OH^- + $OH^{\bullet}$

The degradation of hazardous methylene blue dye (HMBD) through direct oxidation reactions on the surface of photo-catalyst gives the oxidized products:

OH• + HMBD → HMBD• + H_2O

HMBD + h^+ → $HMBD^+$• (degraded products, i.e., NH_4^+, H_2O, CO_2 etc.)

Photo-catalytic activities of the $ZnWO_4$-NPs@rGO nanocomposites were examined by degradation of an HMBD solution under visible-light irradiation at a pH of ~7, and the photo-catalytic degradation data were monitored at the maximum absorption peak (λ_{max}) of ~662 nm by a UV–Vis spectrophotometer. The absorption peak intensities were reduced with time under visible-light irradiations (Figure 6b). The decremental responses in absorption peak intensities of the HMBD solution demonstrates the degradation of HMBD on the surface of the $ZnWO_4$-NPs@rGO nanocomposites. Photo-catalytic efficiencies of the $ZnWO_4$-NPs@rGO nanocomposites acting as photo-catalysts were estimated using the given formula ($\eta = [1-(C_t/C_0)] \times 100\%$), where '$C_0$' and '$C_t$' represent the initial concentration of the HMBD solution, and the concentration after time 't', respectively. The

$ZnWO_4$-NPs@rGO nanocomposites degraded ~98% of the HMBD solution, and almost decolorized the solution in 120 min, while ~52% of HMBD was degraded by pure $ZnWO_4$-NPs in the same time (i.e., 120 min) as shown in Figure 6c. Figure 6d shows a linear plot of the photo-catalytic efficiencies with time vs. $\ln(C_0/C_t)$. The linear plot shows the pseudo first-order kinetic behavior of the photo-catalytic reactions. The rate constant and R^2 values were found to be ~0.016 m^{-1} and ~0.9833, respectively. The photo-catalytic degradations of HMBD were reported to be ~90%, 70%, and 30% with the $ZnWO_4$, $CuWO_4$, and $CoWO_4$ photo-catalysts, respectively, in 120 min [45]. WO_3 nanoparticles were also used as photo-catalysts in the degradation of HMBD, and the degradation of the dye was reported to be ~20% in 160 min [46]. Recently, $ZnWO_4$ nanostructures were significantly used as photo-catalysts in the photo-catalytic degradation of an HMBD solution (i.e., ~85% degradation in 3 h) [1]. Hence, existing work reveals the enhanced photo-catalytic performance of $ZnWO_4$-NPs@rGO nanocomposites in the degradation of HMBD solutions under visible-light irradiations. An ESI-MS spectrometric study of the degraded samples was also undertaken to support our conclusions regarding the photocatalytic degradation reactions of methylene blue dye. Figure 7 shows the ESI-MS spectra of the HMBD solution before and after photo-catalytic degradation. The molecular ion peak of methylene blue dye was reported previously at the m/z peak position of 284 before degradation [2,47]. No spectral line was detected in the mass spectrometric spectrum at the m/z position of 284 after photocatalytic degradation of methylene blue dye. These results indicate that the dye had been oxidized into various intermediates or fragments (i.e., organic molecules), as the spectral lines appeared at various m/z values in the spectrum. This is noteworthy as the intermediates, or fragments of the dye could be generated by the attack of free radicals (i.e., $OH^{\bullet}$ and $O_2^{\bullet -}$) on dye molecules under visible-light irradiations. The intermediates, or fragments, can further degrade into inorganic minerals under longer irradiation times, as also reported elsewhere [48]. Recycling of the $ZnWO_4$-NPs@rGO photo-catalysts is one of the important concerns for industrial applications. The recycled photocatalytic efficiencies of the $ZnWO_4$-NPs@rGO nanocomposites were also examined for eight consecutive cycles under visible-light irradiation. $ZnWO_4$-NPs@rGO nanocomposites show excellent recycled efficiencies for the photo-catalytic degradation of HMBD solutions. We found that regenerated $ZnWO_4$-NPs@rGO photo-catalysts degraded the HMBD solution efficiently for up to eight cycles (Figure 8). Note that the $ZnWO_4$-NPs@rGO photo-catalysts were washed with deionized water several times after each cycle, and then used again for the next cycle repeatedly. Based on the current results, $ZnWO_4$-NPs@rGO nanocomposites work as superior photo-catalysts in water purification applications for environmental remediation.

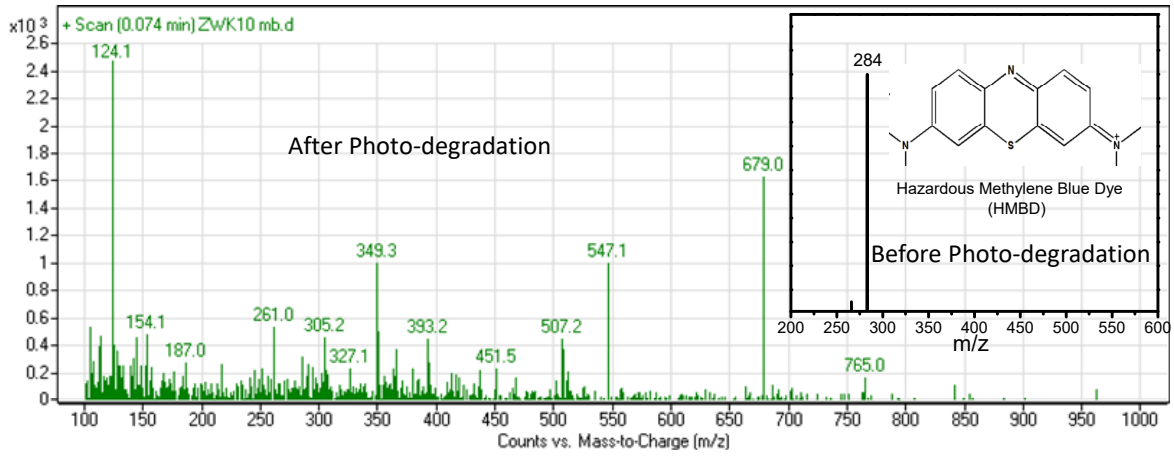

Figure 7. ESI-MS spectra of HMBD solution before and after photo-catalytic degradation.

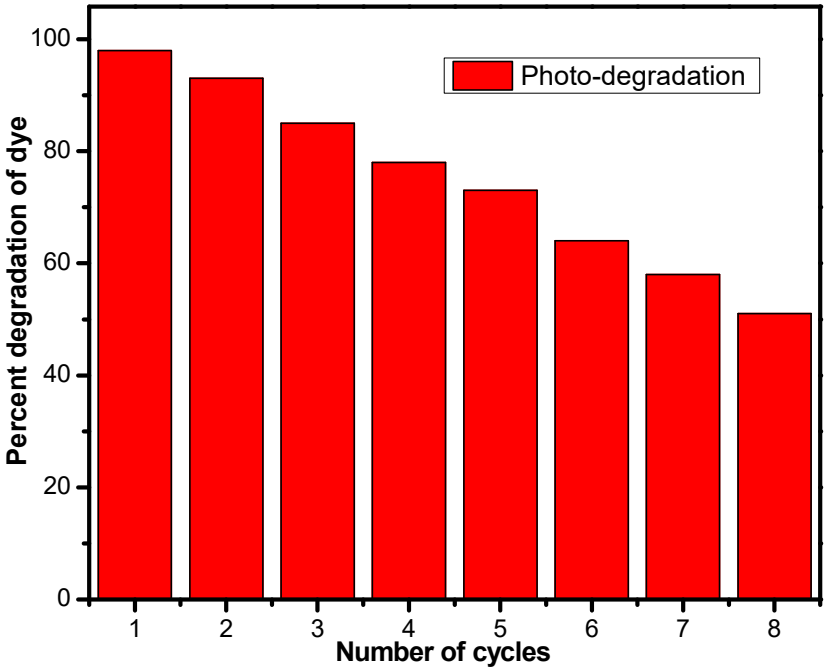

Figure 8. Recycled photocatalytic efficiencies of $ZnWO_4$-NPs@rGO nanocomposites.

4. Conclusions

Hydrothermally synthesized $ZnWO_4$-NPs@rGO nanocomposites were shown to have superior photo-catalytic activities over pure $ZnWO_4$ nanoparticles. The photo-catalytic activities of $ZnWO_4$-NPs@rGO nanocomposites for the degradation of HMBD showed excellent performances with ~98% dye degradation, which is far better than that of pure $ZnWO_4$ photo-catalysts (~53% dye degradation), in 120 min. Hence, $ZnWO_4$-NPs@rGO nanocomposites can be considered as significant photo-catalysts for environmental remediation and energy applications.

Author Contributions: Conceptualization, Data curation, Methodology, Formal analysis, N.A.; supervision, Validation, Project administration, S.M.A.; Investigation, Validation, Project administration, Writing – review & editing, J.A. All authors have read and agreed to the published version of the manuscript.

Funding: This research was funded by Researchers Supporting Project number (RSP-2021/391), King Saud University.

Acknowledgments: The authors extend their sincere appreciation to Researchers Supporting Project at the King Saud University, Riyadh, Saudi Arabia.

Conflicts of Interest: The authors declare no conflict of interest.

References

1. Alshehri, S.M.; Ahmed, J.; Ahamad, T.; Alhokbany, N.; Arunachalam, P.; Al-Mayouf, A.M.; Ahmad, T. Synthesis, characterization, multifunctional electrochemical (OGR/ORR/SCs) and photodegradable activities of $ZnWO_4$ nanobricks. *J. Sol-Gel Sci. Technol.* **2018**, *87*, 137–146. [CrossRef]
2. AlShehri, S.M.; Ahmed, J.; Alzahrani, A.M.; Ahamad, T. Synthesis, characterization, and enhanced photocatalytic properties of $NiWO_4$ nanobricks. *New J. Chem.* **2017**, *41*, 8178–8186. [CrossRef]
3. Amouzegar, Z.; Naghizadeh, R.; Rezaie, H.R.; Ghahari, M.; Aminzare, M. Cubic $ZnWO_4$ nano-photocatalysts synthesized by the microwave-assisted precipitation technique. *Ceram. Int.* **2015**, *41*, 1743–1747. [CrossRef]
4. Barzgari, Z.; Askari, S.Z.; Ghazizadeh, A. Fabrication of nanostructured $CuWO_4$ for photocatalytic degradation of organic pollutants in aqueous solution. *J. Mater. Sci. Mater. Electron.* **2017**, *28*, 3293–3298. [CrossRef]
5. Ahmed, J.; Ahamad, T.; Ubaidullah, M.; Al-Enizi, A.M.; Alhabarah, A.N.; Alhokbany, N.; Alshehri, S.M. rGO supported $NiWO_4$ nanocomposites for hydrogen evolution reactions. *Mater. Lett.* **2019**, *240*, 51–54. [CrossRef]

6. Ahmed, J.; Alhokbany, N.; Ahamad, T.; AlShehri, S.M. Investigation of enhanced electro-catalytic HER/OER performances of copper tungsten oxide@reduced graphene oxide nanocomposites in alkaline and acidic media. *New J. Chem.* **2022**. [CrossRef]
7. Dhilip Kumar, R.; Andou, Y.; Sathish, M.; Karuppuchamy, S. Synthesis of nanostructured Cu-WO_3 and $CuWO_4$ for supercapacitor applications. *J. Mater. Sci. Mater. Electron.* **2016**, *27*, 2926–2932. [CrossRef]
8. Kumar, R.D.; Andou, Y.; Karuppuchamy, S. Synthesis and characterization of nanostructured Ni-WO_3 and $NiWO_4$ for supercapacitor applications. *J. Alloys Compd.* **2016**, *654*, 349–356. [CrossRef]
9. Zheng, Y.; Zheng, L.; Zhan, Y.; Lin, X.; Zheng, Q.; Wei, K. Ag/ZnO Heterostructure Nanocrystals: Synthesis, Characterization, and Photocatalysis. *Inorg. Chem.* **2007**, *46*, 6980–6986. [CrossRef]
10. Yu, C.; Yu, J.C. Sonochemical fabrication, characterization and photocatalytic properties of Ag/$ZnWO_4$ nanorod catalyst. *Mater. Sci. Eng. B* **2009**, *164*, 16–22. [CrossRef]
11. Anandan, S.; Sivasankar, T.; Lana-Villarreal, T. Synthesis of TiO_2/WO_3 nanoparticles via sonochemical approach for the photocatalytic degradation of methylene blue under visible light illumination. *Ultrason. Sonochem.* **2014**, *21*, 1964–1968. [CrossRef]
12. Fujii, A.; Meng, Z.; Yogi, C.; Hashishin, T.; Sanada, T.; Kojima, K. Preparation of Pt-loaded WO_3 with different types of morphology and photocatalytic degradation of methylene blue. *Surf. Coat. Technol.* **2015**, *271*, 251–258. [CrossRef]
13. Keereeta, Y.; Thongtem, S.; Thongtem, T. Enhanced photocatalytic degradation of methylene blue by WO_3/$ZnWO_4$ composites synthesized by a combination of microwave-solvothermal method and incipient wetness procedure. *Powder Technol.* **2015**, *284*, 85–94. [CrossRef]
14. Sivaganesh, D.; Saravanakumar, S.; Sivakumar, V.; Rajajeyaganthan, R.; Arunpandian, M.; Nandha Gopal, J.; Thirumalaisamy, T.K. Surfactants-assisted synthesis of $ZnWO_4$ nanostructures: A view on photocatalysis, photoluminescence and electron density distribution analysis. *Mater. Charact.* **2020**, *159*, 110035. [CrossRef]
15. Fu, H.; Lin, J.; Zhang, L.; Zhu, Y. Photocatalytic activities of a novel $ZnWO_4$ catalyst prepared by a hydrothermal process. *Appl. Catal. A Gen.* **2006**, *306*, 58–67. [CrossRef]
16. Huang, G.; Zhang, C.; Zhu, Y. $ZnWO_4$ photocatalyst with high activity for degradation of organic contaminants. *J. Alloys Compd.* **2007**, *432*, 269–276. [CrossRef]
17. Fu, H.; Pan, C.; Zhang, L.; Zhu, Y. Synthesis, characterization and photocatalytic properties of nanosized Bi_2WO_6, $PbWO_4$ and $ZnWO_4$ catalysts. *Mater. Res. Bull.* **2007**, *42*, 696–706. [CrossRef]
18. Garadkar, K.M.; Ghule, L.A.; Sapnar, K.B.; Dhole, S.D. A facile synthesis of $ZnWO_4$ nanoparticles by microwave assisted technique and its application in photocatalysis. *Mater. Res. Bull.* **2013**, *48*, 1105–1109. [CrossRef]
19. Hosseinpour-Mashkani, S.M.; Maddahfar, M.; Sobhani-Nasab, A. Precipitation Synthesis, Characterization, Morphological Control, and Photocatalyst Application of $ZnWO_4$ Nanoparticles. *J. Electron. Mater.* **2016**, *45*, 3612–3620. [CrossRef]
20. Leonard, K.C.; Nam, K.M.; Lee, H.C.; Kang, S.H.; Park, H.S.; Bard, A.J. $ZnWO_4$/WO_3 Composite for Improving Photoelectrochemical Water Oxidation. *J. Phys. Chem. C* **2013**, *117*, 15901–15910. [CrossRef]
21. Li, M.; Zhu, Q.; Li, J.-G.; Kim, B.-N. Elongation of $ZnWO_4$ nanocrystals for enhanced photocatalysis and the effects of Ag decoration. *Appl. Surf. Sci.* **2020**, *515*, 146011. [CrossRef]
22. Dumrongrojthanath, P.; Phuruangrat, A.; Thongtem, S.; Thongtem, T. Facile sonochemical synthesis and photocatalysis of Ag nanoparticle/$ZnWO_4$-nanorod nanocomposites. *Rare Met.* **2019**, *38*, 601–608. [CrossRef]
23. He, H.; Luo, Z.; Yu, C. Multifunctional $ZnWO_4$ nanoparticles for photocatalytic removal of pollutants and disinfection of bacteria. *J. Photochem. Photobiol. A Chem.* **2020**, *401*, 112735. [CrossRef]
24. He, H.; Luo, Z.; Tang, Z.-Y.; Yu, C. Controllable construction of $ZnWO_4$ nanostructure with enhanced performance for photosensitized Cr(VI) reduction. *Appl. Surf. Sci.* **2019**, *490*, 460–468. [CrossRef]
25. Zhao, Z.; Zhang, B.; Chen, D.; Guo, Z.; Peng, Z. Simultaneous Reduction of Vanadium (V) and Chromium (VI) in Wastewater by Nanosized $ZnWO_4$ Photocatalysis. *J. Nanosci. Nanotechnol.* **2016**, *16*, 2847–2852. [CrossRef]
26. Li, M.; Wang, X.; Zhu, Q.; Li, J.-G.; Kim, B.-N. Crystallization and architecture engineering of $ZnWO_4$ for enhanced photoluminescence. *CrystEngComm* **2020**, *22*, 6398–6406. [CrossRef]
27. Brijesh, K.; Vinayraj, S.; Dhanush, P.C.; Bindu, K.; Nagaraja, H.S. $ZnWO_4$/SnO_2@r-GO nanocomposite as an anode material for high capacity lithium ion battery. *Electrochim. Acta* **2020**, *354*, 136676. [CrossRef]
28. Brijesh, K.; Nagaraja, H.S. $ZnWO_4$/r-GO nanocomposite as high capacity anode for lithium-ion battery. *Ionics* **2020**, *26*, 2813–2823. [CrossRef]
29. Harichandran, G.; Divya, P.; Yesuraj, J.; Muthuraaman, B. Sonochemical synthesis of chain-like $ZnWO_4$ nanoarchitectures for high performance supercapacitor electrode application. *Mater. Charact.* **2020**, *167*, 110490. [CrossRef]
30. Vinayaraj, S.; Brijesh, K.; Dhanush, P.C.; Nagaraja, H.S. $ZnWO_4$/SnO_2 composite for supercapacitor applications. *Physica B Condens. Matter.* **2020**, *596*, 412369. [CrossRef]
31. Yan, X.; Ohno, T.; Nishijima, K.; Abe, R.; Ohtani, B. Is methylene blue an appropriate substrate for a photocatalytic activity test? A study with visible-light responsive titania. *Chem. Phys. Lett.* **2006**, *429*, 606–610. [CrossRef]
32. Ohtani, B. Photocatalysis A to Z—What we know and what we do not know in a scientific sense. *J. Photochem. Photobiol. C Photochem. Rev.* **2010**, *11*, 157–178. [CrossRef]
33. Ahmed, J.; Ahamad, T.; Alhokbany, N.; Almaswari, B.M.; Ahmad, T.; Hussain, A.; Al-Farraj, E.S.S.; Alshehri, S.M. Molten Salts Derived Copper Tungstate Nanoparticles as Bifunctional Electro-Catalysts for Electrolysis of Water and Supercapacitor Applications. *ChemElectroChem* **2018**, *5*, 3938–3945. [CrossRef]

34. Ahmed, J.; Poltavets, V.V.; Prakash, J.; Alshehri, S.M.; Ahamad, T. Sol–gel synthesis, structural characterization and bifunctional catalytic activity of nanocrystalline delafossite $CuGaO_2$ particles. *J. Alloys Compd.* **2016**, *688*, 1157–1161. [CrossRef]
35. Ahmed, J.; Ubiadullah, M.; Alhokbany, N.; Alshehri, S.M. Synthesis of ultrafine $NiMoO_4$ nano-rods for excellent electro-catalytic performance in hydrogen evolution reactions. *Mater. Lett.* **2019**, *257*, 126696. [CrossRef]
36. AlShehri, S.M.; Ahmed, J.; Ahamad, T.; Arunachalam, P.; Ahmad, T.; Khan, A. Bifunctional electro-catalytic performances of $CoWO_4$ nanocubes for water redox reactions (OER/ORR). *RSC Adv.* **2017**, *7*, 45615–45623. [CrossRef]
37. Ahmed, J.; Alam, M.; Majeed Khan, M.A.; Alshehri, S.M. Bifunctional electro-catalytic performances of $NiMoO_4$-NRs@RGO nanocomposites for oxygen evolution and oxygen reduction reactions. *J. King Saud Univ. Sci.* **2021**, *33*, 101317. [CrossRef]
38. Alshehri, S.M.; Ahmed, J.; Alhabarah, A.N.; Ahamad, T.; Ahmad, T. Nitrogen-Doped Cobalt Ferrite/Carbon Nanocomposites for Supercapacitor Applications. *ChemElectroChem* **2017**, *4*, 2952–2958. [CrossRef]
39. Huang, K.; Li, Y.H.; Lin, S.; Liang, C.; Wang, H.; Ye, C.X.; Wang, Y.J.; Zhang, R.; Fan, D.Y.; Yang, H.J.; et al. A facile route to reduced graphene oxide–zinc oxide nanorod composites with enhanced photocatalytic activity. *Powder Technol.* **2014**, *257*, 113–119. [CrossRef]
40. Zhao, D.; Zhou, Y.; Deng, Y.; Xiang, Y.; Zhang, Y.; Zhao, Z.; Zeng, D. A Novel and Reusable RGO/ZnO with Nanosheets/Microparticle Composite Photocatalysts for Efficient Pollutants Degradation. *ChemistrySelect* **2018**, *3*, 8740–8747. [CrossRef]
41. Liu, S.; Sun, H.; Suvorova, A.; Wang, S. One-pot hydrothermal synthesis of ZnO-reduced graphene oxide composites using Zn powders for enhanced photocatalysis. *Chem. Eng. J.* **2013**, *229*, 533–539. [CrossRef]
42. Ahmed, J.; Ubiadullah, M.; Khan, M.A.M.; Alhokbany, N.; Alshehri, S.M. Significant recycled efficiency of multifunctional nickel molybdenum oxide nanorods in photo-catalysis, electrochemical glucose sensing and asymmetric supercapacitors. *Mater. Charact.* **2021**, *171*, 110741. [CrossRef]
43. Tauc, J. Optical properties and electronic structure of amorphous Ge and Si. *Mater. Res. Bull.* **1968**, *3*, 37–46. [CrossRef]
44. Zhang, C.; Zhang, H.; Zhang, K.; Li, X.; Leng, Q.; Hu, C. Photocatalytic Activity of $ZnWO_4$: Band Structure, Morphology and Surface Modification. *ACS Appl. Mater. Interfaces* **2014**, *6*, 14423–14432. [CrossRef] [PubMed]
45. Montini, T.; Gombac, V.; Hameed, A.; Felisari, L.; Adami, G.; Fornasiero, P. Synthesis, characterization and photocatalytic performance of transition metal tungstates. *Chem. Phys. Lett.* **2010**, *498*, 113–119. [CrossRef]
46. Ahmed, B.; Kumar, S.; Ojha, A.K.; Donfack, P.; Materny, A. Facile and controlled synthesis of aligned WO_3 nanorods and nanosheets as an efficient photocatalyst material. *Spectrochim. Acta Part A Mol. Biomol. Spectrosc.* **2017**, *175*, 250–261. [CrossRef]
47. Molla, A.; Sahu, M.; Hussain, S. Under dark and visible light: Fast degradation of methylene blue in the presence of Ag-In-Ni-S nanocomposites. *J. Mater. Chem. A* **2015**, *3*, 15616–15625. [CrossRef]
48. Houas, A.; Lachheb, H.; Ksibi, M.; Elaloui, E.; Guillard, C.; Herrmann, J.-M. Photocatalytic degradation pathway of methylene blue in water. *Appl. Catal. B Environ.* **2001**, *31*, 145–157. [CrossRef]